13

Lateral Earth Pressure—Curved Failure Surface

In Chapter 12, we considered Coulomb's earth pressure theory, in which the retaining wall was considered to be rough. The potential failure surfaces in the backfill were considered to be planes. In reality, most failure surfaces in soil are curved. There are several instances where the assumption of plane failure surfaces in soil may provide unsafe results. Examples of these cases are the estimation of passive pressure and braced cuts. This chapter describes procedures by which passive earth pressure and lateral earth pressure on braced cuts can be estimated using curved failure surfaces in the soil.

13.1 Retaining Walls with Friction

In reality, retaining walls are rough, and shear forces develop between the face of the wall and the backfill. To understand the effect of wall friction on the failure surface, let us consider a rough retaining wall AB with a horizontal granular backfill as shown in Figure 13.1.

In the active case (Figure 13.1a), when the wall AB moves to a position $A'B$, the soil mass in the active zone will be stretched outward. This will cause a downward motion of the soil relative to the wall. This motion causes a downward shear on the wall (Figure 13.1b), and it is called a *positive wall friction in the active case.* If δ is the angle of friction between the wall and the backfill, then the resultant active force P_a will be inclined at an angle δ to the normal drawn to the back face of the retaining wall. Advanced studies show that the failure surface in the backfill can be represented by BCD, as shown in Figure 13.1a. The portion BC is curved, and the portion CD of the failure surface is a straight line. Rankine's active state exists in the zone ACD.

Under certain conditions, if the wall shown in Figure 13.1a is forced downward with reference to the backfill, the direction of the active force P_a will change as shown in Figure 13.1c. This is a situation of negative wall friction $(-\delta)$ in the active case. Figure 13.1c also shows the nature of the failure surface in the backfill.

The effect of wall friction for the passive state is shown in Figures 13.1d and e. When the wall AB is pushed to a position $A'B$ (Figure 13.1d), the soil in the passive

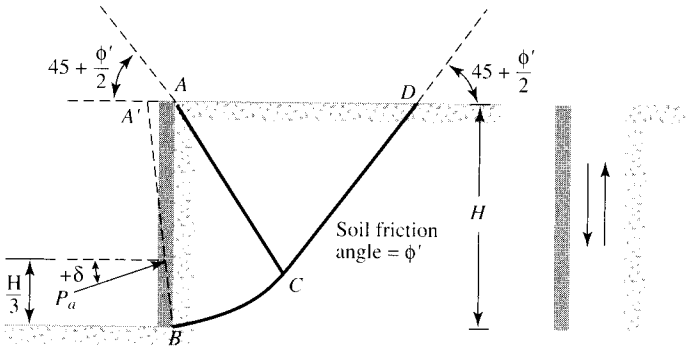

(a) Active case (+δ) (b)

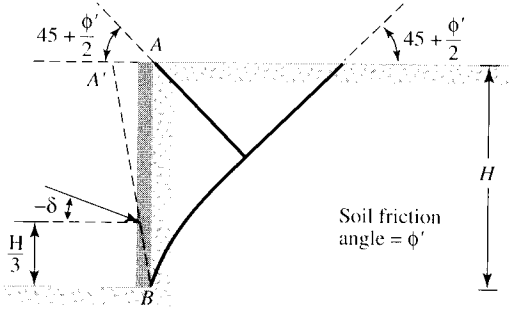

(c) Active case (−δ)

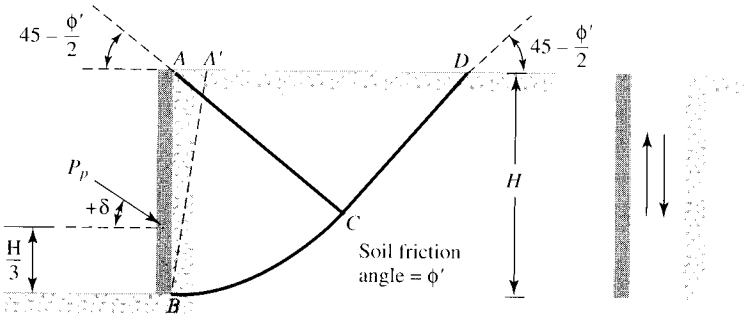

(d) Passive case (+δ) (e)

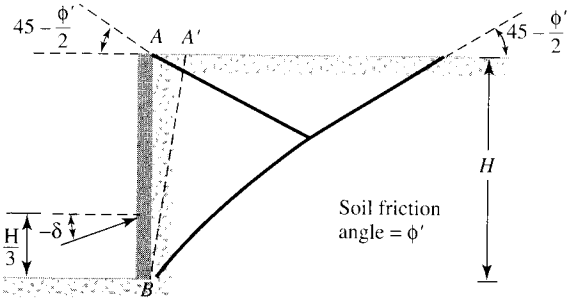

(f) Passive case (−δ)

Figure 13.1 Effect of wall friction on failure surface

zone will be compressed. The result is an upward motion relative to the wall. The upward motion of the soil will cause an upward shear on the retaining wall (Figure 13.1e). This is referred to as *positive wall friction in the passive case.* The resultant passive force, P_p, will be inclined at an angle δ to the normal drawn to the back face of the wall. The failure surface in the soil has a curved lower portion BC and a straight upper portion CD. Rankine's passive state exists in the zone ACD.

If the wall shown in Figure 13.1d is forced upward relative to the backfill by a force, then the direction of the passive force P_p will change as shown in Figure 13.1f. This is *negative wall friction in the passive case* $(-\delta)$. Figure 13.1f also shows the nature of the failure surface in the backfill under such a condition.

For practical considerations, in the case of loose granular backfill, the angle of wall friction δ is taken to be equal to the angle of friction of soil, ϕ'. For dense granular backfills, δ is smaller than ϕ' and is in the range of $\phi'/2 \leq \delta \leq (2/3)\phi'$.

The assumption of plane failure surface gives reasonably good results while calculating active earth pressure. However, the assumption that the failure surface is a plane in Coulomb's theory grossly overestimates the passive resistance of walls, particularly for $\delta > \phi'/2$.

13.2 Properties of a Logarithmic Spiral

The case of passive pressure shown in Figure 13.1d (case of $+\delta$) is the most common one encountered in design and construction. Also, the curved failure surface represented by BC in Figure 13.1d is most commonly assumed to be the arc of a logarithmic spiral. In a similar manner, the failure surface in soil in the case of braced cuts (Sections 13.6 to 13.10) is also assumed to be the arc of a logarithmic spiral. Hence, some useful ideas concerning the properties of a logarithmic spiral are described in this section.

The equation of the logarithmic spiral generally used in solving problems in soil mechanics is of the form

$$r = r_o e^{\theta \tan \phi'} \tag{13.1}$$

where r = radius of the spiral
r_o = starting radius at $\theta = 0$
ϕ' = angle of friction of soil
θ = angle between r and r_o

The basic parameters of a logarithmic spiral are shown in Figure 13.2, in which O is the center of the spiral. The area of the sector OAB is given by

$$A = \int_0^{\theta} \frac{1}{2} r(r\, d\theta) \tag{13.2}$$

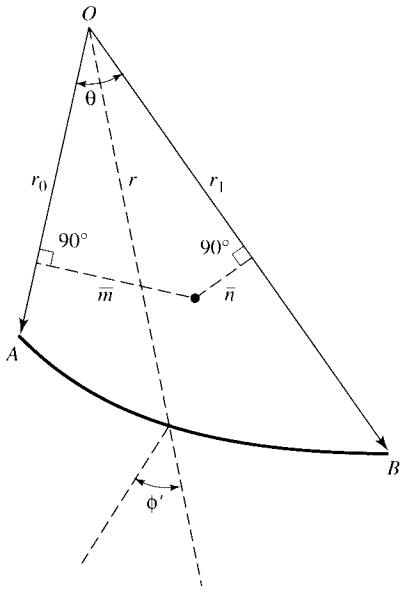

Figure 13.2
General parameters of a logarithmic spiral

Substituting the values of r from Eq. (13.1) into Eq. (13.2), we get

$$A = \int_0^{\theta_1} \frac{1}{2} r_o^2 e^{2\theta \tan \phi'} \, d\theta$$

$$= \frac{r_1^2 - r_o^2}{4 \tan \phi'} \tag{13.3}$$

The location of the centroid can be defined by the distances $\bar{m}$ and $\bar{n}$ (Figure 13.2), measured from OA and OB, respectively, and can be given by the following equations (Hijab, 1956):

$$\bar{m} = \frac{4}{3} r_o \frac{\tan \phi'}{(9 \tan^2 \phi' + 1)} \left[\frac{\left(\frac{r_1}{r_o}\right)^3 (3 \tan \phi' \sin \theta - \cos \theta) + 1}{\left(\frac{r_1}{r_o}\right)^2 - 1} \right] \tag{13.4}$$

$$\bar{n} = \frac{4}{3} r_o \frac{\tan \phi'}{(9 \tan^2 \phi' + 1)} \left[\frac{\left(\frac{r_1}{r_o}\right)^3 - 3 \tan \phi' \sin \theta - \cos \theta}{\left(\frac{r_1}{r_o}\right)^2 - 1} \right] \tag{13.5}$$

Another important property of the logarithmic spiral defined by Eq. (13.1) is that any radial line makes an angle ϕ' with the normal to the curve drawn at the point

where the radial line and the spiral intersect. This basic property is particularly useful in solving problems related to lateral earth pressure.

PASSIVE EARTH PRESSURE

13.3 Procedure for Determination of Passive Earth Pressure, P_p (Cohesionless Backfill)

Figure 13.1d shows the curved failure surface in the granular backfill of a retaining wall of height H. The shear strength of the granular backfill is expressed as

$$\tau_f = \sigma' \tan \phi' \tag{13.6}$$

The curved lower portion BC of the failure wedge is an arc of a logarithmic spiral defined by Eq. (13.1). The center of the log spiral lies on the line CA (not necessarily within the limits of points C and A). The upper portion CD is a straight line that makes an angle of $(45 - \phi'/2)$ degrees with the horizontal. The soil in the zone ACD is in *Rankine's passive state.*

Figure 13.3 shows the procedure for evaluating the passive resistance by trial wedges (Terzaghi and Peck, 1967). The retaining wall is first drawn to scale as shown in Figure 13.3a. The line C_1A is drawn in such a way that it makes an angle of $(45 - \phi'/2)$ degrees with the surface of the backfill. BC_1D_1 is a trial wedge in which BC_1 is the arc of a logarithmic spiral. According to the equation $r_1 = r_o e^{\theta \tan \phi'}$, O_1 is the center of the spiral. (*Note:* $\overline{O_1B} = r_o$ and $\overline{O_1C_1} = r_1$ and $\angle BO_1C_1 = \theta_1$; refer to Figure 13.2.)

Now let us consider the stability of the soil mass ABC_1C_1' (Figure 13.3b). For equilibrium, the following forces per unit length of the wall are to be considered:

1. Weight of the soil in zone $ABC_1C_1' = W_1 = (\gamma)(\text{Area of } ABC_1C_1')(1)$.
2. The vertical face, C_1C_1', is in the zone of Rankine's passive state; hence, the force acting on this face is

$$P_{d(1)} = \frac{1}{2}\gamma(d_1)^2 \tan^2\left(45 + \frac{\phi'}{2}\right) \tag{13.7}$$

   where $d_1 = \overline{C_1C_1'}$. $P_{d(1)}$ acts horizontally at a distance of $d_1/3$ measured vertically upward from C_1.
3. F_1 is the resultant of the shear and normal forces that act along the surface of sliding, BC_1. At any point on the curve, according to the property of the logarithmic spiral, a radial line makes an angle ϕ' with the normal. Because the resultant, F_1, makes an angle ϕ' with the normal to the spiral at its point of application, its line of application will coincide with a radial line and will pass through the point O_1.
4. P_1 is the passive force per unit length of the wall. It acts at a distance of $H/3$ measured vertically from the bottom of the wall. The direction of the force P_1 is inclined at an angle δ with the normal drawn to the back face of the wall.

Now, taking the moments of W_1, $P_{d(1)}$, F_1, and P_1 about the point O_1, for equilibrium, we have

$$W_1[l_{W(1)}] + P_{d(1)}[l_1] + F_1[0] = P_1[l_{P(1)}] \tag{13.8}$$

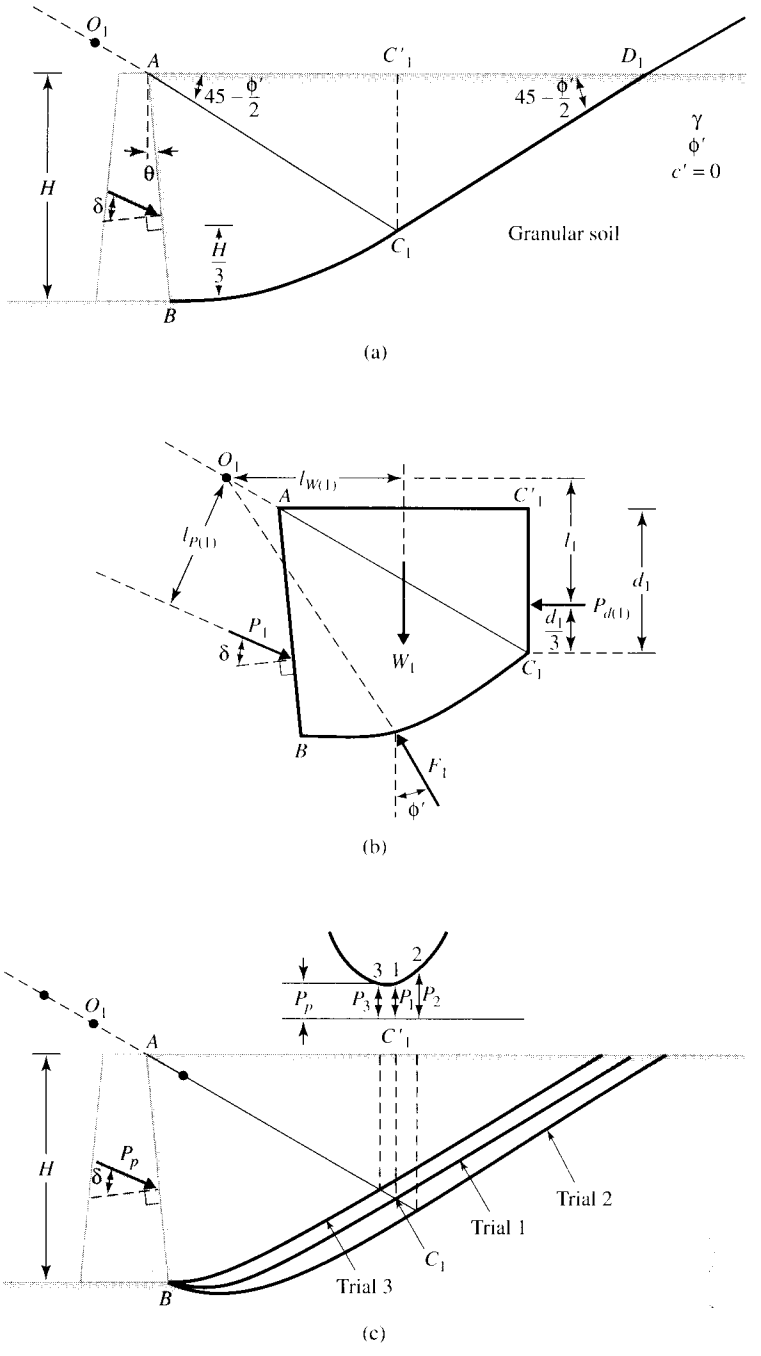

Figure 13.3 Passive earth pressure against retaining wall with curved failure surface

or

$$P_1 = \frac{1}{l_{P(1)}}[W_1 l_{W(1)} + P_{d(1)} l_1] \tag{13.9}$$

where $l_{W(1)}$, l_1, and $l_{P(1)}$ are moment arms for the forces W_1, $P_{d(1)}$, and P_1, respectively.

The preceding procedure for finding the trial passive force per unit length of the wall is repeated for several trial wedges such as those shown in Figure 13.3c. Let $P_1, P_2, P_3, \ldots, P_n$ be the forces that correspond to trial wedges $1, 2, 3, \ldots, n$, respectively. The forces are plotted to some scale as shown in the upper part of the figure. A smooth curve is plotted through the points $1, 2, 3, \ldots, n$. The lowest point of the smooth curve defines the actual passive force, P_p, per unit length of the wall.

13.4 Coefficient of Passive Earth Pressure (K_p)

The passive force per unit length of a rough retaining wall with a cohesionless horizontal backfill can be calculated as

$$P_p = \frac{1}{2}\gamma H_1^2 K_p \tag{13.10}$$

where K_p = passive pressure coefficient.

For the definition of H_1, see Figure 13.4. The variation of K_p determined by Caquot and Kerisel (1948) is also shown in Figure 13.4.

It is important to note that the K_p values shown in Figure 13.4 are for $\delta/\phi' = 1$. If $\delta/\phi' \neq 1$, the following procedure must be used to determine K_p:

1. Assume δ and ϕ'.
2. Calculate δ/ϕ'.
3. Using the ratio of δ/ϕ' (step 2), determine the reduction factor, R, from Table 13.1.
4. Determine K_p from Figure 13.4 for $\delta/\phi' = 1$.
5. Calculate K_p for the required δ/ϕ' as

$$K_p = (R)[K_{p(\delta/\phi'=1)}] \tag{13.11}$$

Shields and Tolunay (1973) improved the trial wedge solution described in Section 13.3 by using the *method of slices* to consider the stability of the trial soil wedge such as ABC_1C_1' in Figure 13.3a. The details of the analysis are beyond the scope of this text. However, the values of K_p (passive earth pressure coefficient) obtained by this method are given in Table 13.2, and they seem to be as good as any other set of values available currently. Note that the values of K_p shown in Table 13.1 are for retaining walls with a vertical back (that is, $\theta = 0$ in Figure 13.3) supporting a granular backfill with a horizontal ground surface. The passive pressure for such a case can be given as

$$P_p = \frac{1}{2}\gamma H^2 K_p$$

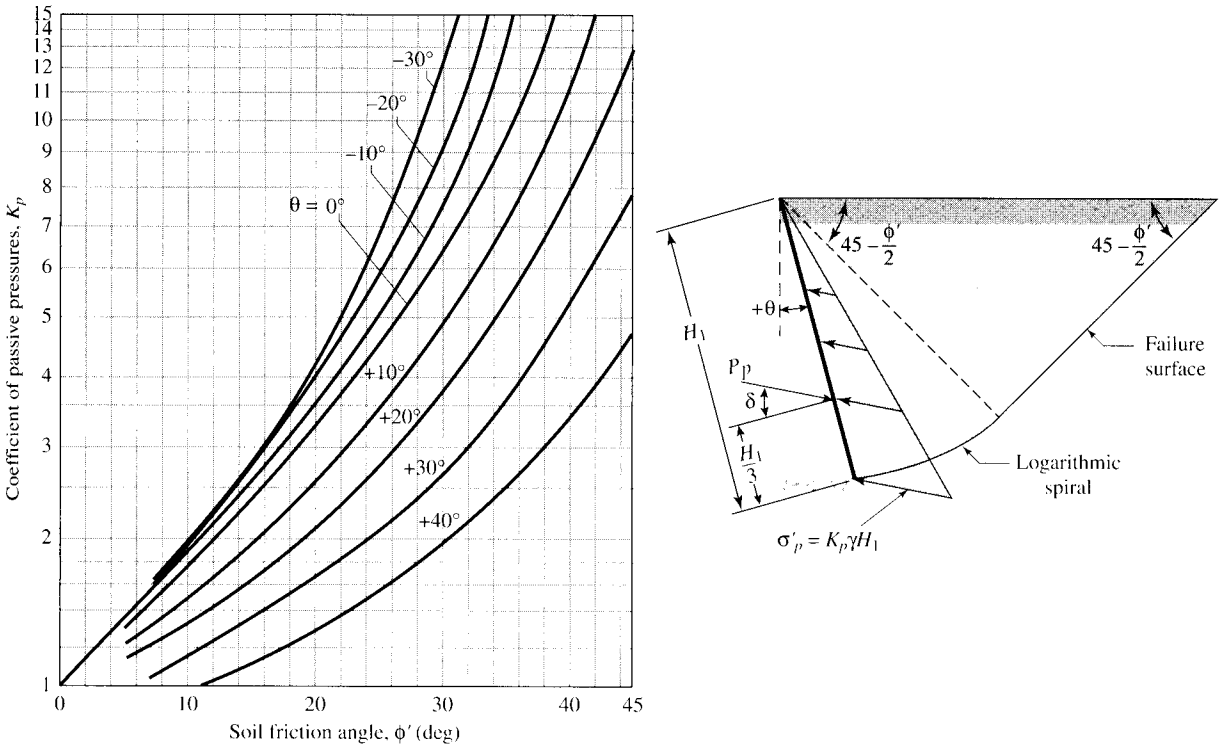

Figure 13.4 Caquot and Kerisel's solution for K_p

Table 13.1 Caquot and Kerisel's Reduction Factor, R, for Passive Pressure Calculation

	δ/ϕ'							
ϕ'	**0.7**	**0.6**	**0.5**	**0.4**	**0.3**	**0.2**	**0.1**	**0.0**
10	0.978	0.962	0.946	0.929	0.912	0.898	0.881	0.864
15	0.961	0.934	0.907	0.881	0.854	0.830	0.803	0.775
20	0.939	0.901	0.862	0.824	0.787	0.752	0.716	0.678
25	0.912	0.860	0.808	0.759	0.711	0.666	0.620	0.574
30	0.878	0.811	0.746	0.686	0.627	0.574	0.520	0.467
35	0.836	0.752	0.674	0.603	0.536	0.475	0.417	0.362
40	0.783	0.682	0.592	0.512	0.439	0.375	0.316	0.262
45	0.718	0.600	0.500	0.414	0.339	0.276	0.221	0.174

Table 13.2 Shields and Tolunay's Values of K_p Based on the Method of Slices

	δ (deg)									
ϕ' (deg)	**0**	**5**	**10**	**15**	**20**	**25**	**30**	**35**	**40**	**45**
20	2.04	2.26	2.43	2.55	2.70					
25	2.46	2.77	3.03	3.23	3.39	3.63				
30	3.00	3.43	3.80	4.13	4.40	4.64	5.03			
35	3.69	4.29	4.84	5.34	5.80	6.21	6.59	7.25		
40	4.69	5.44	6.26	7.05	7.80	8.51	9.18	9.83	11.03	
45	5.83	7.06	8.30	9.55	10.80	12.04	13.26	14.46	15.60	18.01

Example 13.1

Consider a 3-m-high (H) retaining wall with a vertical back ($\theta = 0°$) and a horizontal granular backfill. Given: $\gamma = 15.7$ kN/m^3, $\delta = 15°$, and $\phi' = 30°$. Estimate the passive force, P_p, by using

a. Coulomb's theory
b. curved failure surface assumption (Caquot and Kerisel solution)
c. Shields and Tolunay's solutions

Solution

a. From Eq. (12.89),

$$P_p = \tfrac{1}{2}K_p\gamma H^2$$

From Table 12.7, for $\phi' = 30°$ and $\delta = 15°$, the value of K_p is 4.977. Thus,

$$P = (\tfrac{1}{2})(4.977)(15.7)(3)^2 = \mathbf{351.6\ kN/m}$$

b. From Eq. (13.10),

$$P_p = \tfrac{1}{2}K_p\gamma H_1^2 = \tfrac{1}{2}K_p\gamma H^2 \qquad \text{(because } \theta = 0°,\ H = H_1\text{)}$$

From Figure 13.4, for $\theta = 0°$, $\delta/\phi' = 1$, and $\phi' = 30°$, the value of K_p is 6.4. From Table 13.1, for $\delta/\phi' = 15/30 = 0.5$, the reduction factor, R, is 0.746. Thus, per Eq. (13.11),

$$K_p = (0.746)(6.4) = 4.77$$

So

$$P_p = \tfrac{1}{2}(4.77)(15.7)(3)^2 = \mathbf{337\ kN/m^3}$$

c. $P_p = \dfrac{1}{2}K_p\gamma H^2$

From Table 13.2, for $\phi' = 30°$ and $\delta = 15°$, the value of K_p is 4.13. Hence,

$$P_p = \left(\frac{1}{2}\right)(4.13)(15.7)(3)^2 \approx \mathbf{292\ kN/m}$$ ■

13.5 Passive Force on Walls with Earthquake Forces

The passive force on retaining walls with earthquake forces was discussed in Section 12.15. In that analysis, the backfill was considered to be a granular soil, and the failure surface in the backfill was assumed to be a plane. It was shown in Sections 13.3

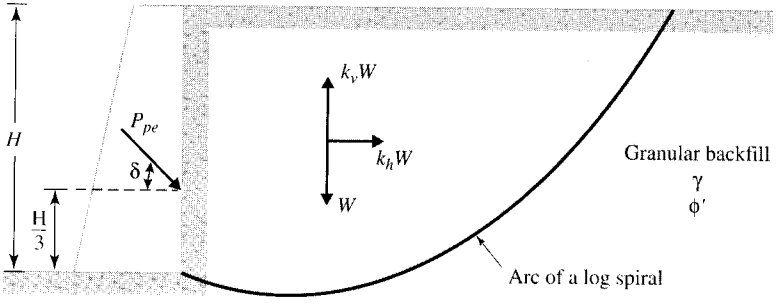

Figure 13.5 Logarithmic spiral failure surface for determination of P_{pe}

and 13.4 that for static conditions and when $\delta > \phi'/2$, the passive force calculated by assuming a plane failure surface in the backfill becomes unsafe. For that reason, Morrison and Ebeling (1995) assumed that the failure surface was an arc of a logarithmic spiral as defined by Eq. (13.1), and they calculated the magnitude of passive force by including earthquake forces (Figure 13.5). In Figure 13.5, the back face of the retaining wall is *vertical* and the backfill is *horizontal.* Also,

H = height of retaining wall

W = weight of failure wedge

P_{pe} = Passive force per unit length of the wall

δ = angle of wall friction

$$k_h = \frac{\text{horizontal component of earthquake acceleration}}{\text{acceleration due to gravity, } g}$$

$$k_v = \frac{\text{vertical component of earthquake acceleration}}{\text{acceleration due to gravity, } g}$$

Based on Morrison and Ebeling's analysis, the passive force can be given as

$$P_{pe} = \frac{1}{2}\gamma H^2 K'_p \tag{13.12}$$

Figure 13.6 shows variation of K'_p with k_h and ϕ' for the Mononobe–Okabe solution [Eq. (12.92)] and for the logarithmic spiral type of failure surface analysis, with $\delta = 2\phi'/3$, $k_v = 0$, $\theta = 0°$, and $\alpha = 0°$. As we can see from the figure, for a given value of k_h, the magnitude of K'_p is always larger when the failure surface is assumed to be a plane (Mononobe–Okabe solution). This is true for all values of ϕ'. Figure 13.7 shows the variation of K'_p with k_h and δ for the Mononobe–Okabe solution and the logarithmic spiral solution, with $k_v = 0$, $\phi' = 30°$, $\theta = 0°$, $\alpha = 0°$, and $\delta = 0, \phi'/2, 2\phi'/3$, and ϕ'.

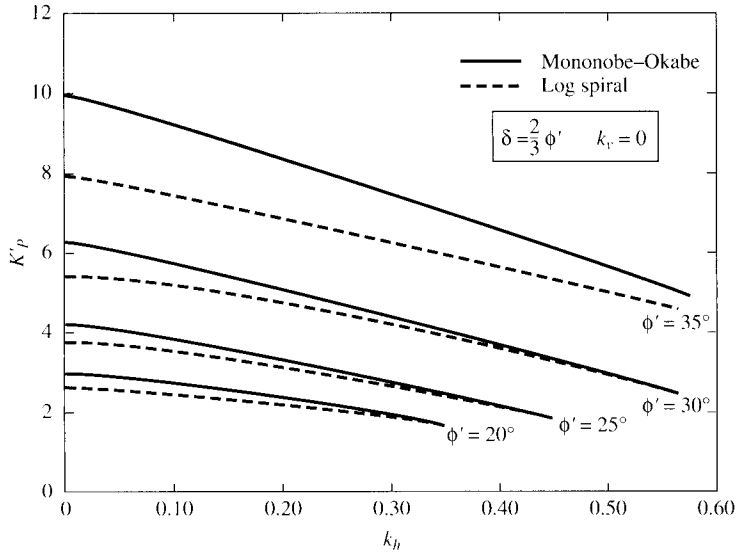

Figure 13.6
Variation of K'_p with k_h and ϕ' ($\delta = \frac{2}{3}\phi'$, $k_v = 0$, $\theta = 0°$, and $\alpha = 0°$) (based on Morrison and Ebeling, 1995)

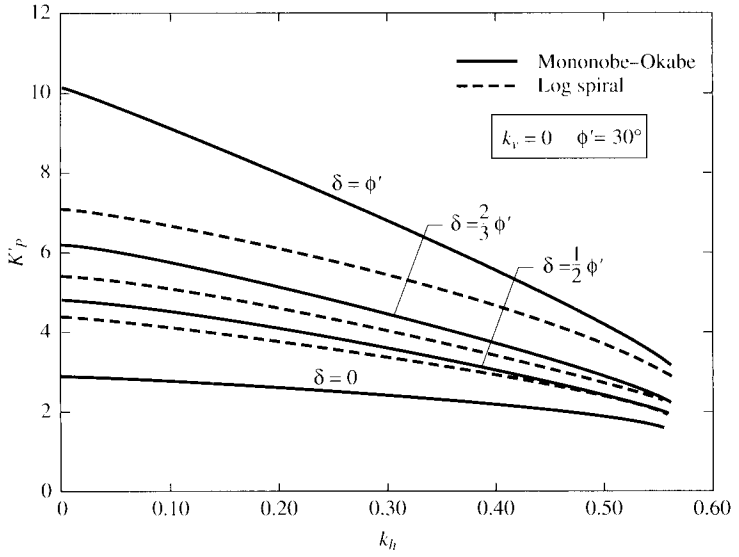

Figure 13.7
Variation of K'_p with k_h and δ ($k_v = 0$, $\phi' = 30°$, $\theta = 0°$, $\alpha = 0°$) (based on Morrison and Ebeling, 1995)

BRACED CUTS

13.6 Braced Cuts—General

Frequently during the construction of foundations or utilities (such as sewers), open trenches with vertical soil slopes are excavated. Although most of these trenches are temporary, the sides of the cuts must be supported by proper bracing systems. Figure 13.8 shows one of several bracing systems commonly adopted in construction practice. The bracing consists of sheet piles, wales, and struts.

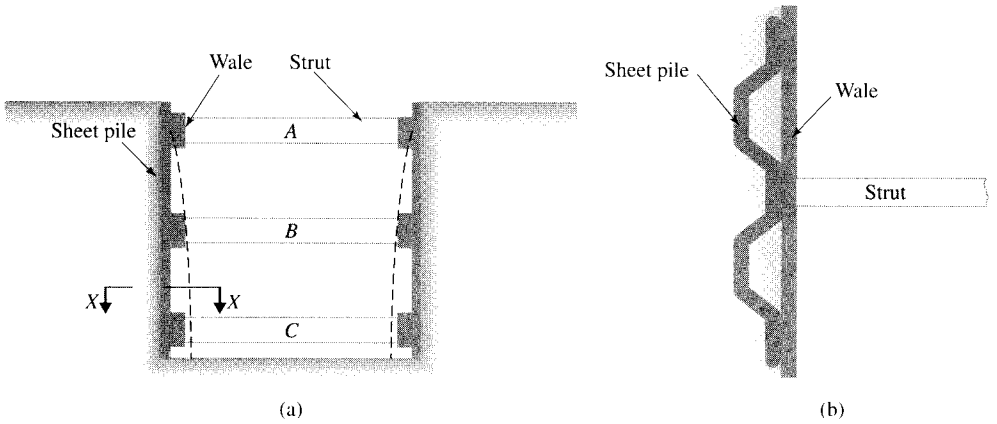

Figure 13.8 Braced cut: (a) cross section; (b) plan (section at X-X)

Proper design of these elements requires a knowledge of the lateral earth pressure exerted on the braced walls. The magnitude of the lateral earth pressure at various depths of the cut is very much influenced by the deformation condition of the sheeting. To understand the nature of the deformation of the braced walls, one needs to follow the sequence of construction. Construction of the unit begins with driving the sheetings. The top row of the wales and struts (marked A in Figure 13.8a) is emplaced immediately after a small cut is made. This emplacement must be done immediately so that the soil mass outside the cut has no time to deform and cause the sheetings to yield. As the sequence of driving the sheetings, excavating the soil, and placing rows of wales and struts (see B and C in Figure 13.8) continues, the sheetings move inward at greater depths. This action is caused by greater earth pressure exerted by the soil outside the cut. The deformation of the braced walls is shown by the broken lines in Figure 13.8a. Essentially, the problem models a condition where the walls are rotating about the level of the top row of struts. A photograph of braced cuts made for subway construction in Chicago is shown in Figure 13.9a. Figures 13.9b and 13.9c are photographs of two braced cuts — one in Seoul, South Korea, and the other in Taiwan.

The deformation of a braced wall differs from the deformation condition of a retaining wall in that, in a braced wall, the rotation is about the top. For this reason, neither Coulomb's nor Rankine's theory will give the actual earth pressure distribution. This fact is illustrated in Figure 13.10 on page 433, in which AB is a frictionless wall with a granular soil backfill. When the wall deforms to position AB', failure surface BC develops. Because the upper portion of the soil mass in the zone ABC does not undergo sufficient deformation, it does not pass into Rankine's active state. The sliding surface BC intersects the ground surface almost at 90°. The corresponding earth pressure will be somewhat parabolic, like *acb* shown in Figure 13.10b. With this type of pressure distribution, the point of application of the resultant active thrust P_a, will be at a height of $n_a H$ measured from the bottom of the wall, with $n_a > \frac{1}{3}$ (for triangular pressure distribution $n_a = \frac{1}{3}$). Theoretical evaluation and field measurements have shown that n_a could be as high as 0.55.

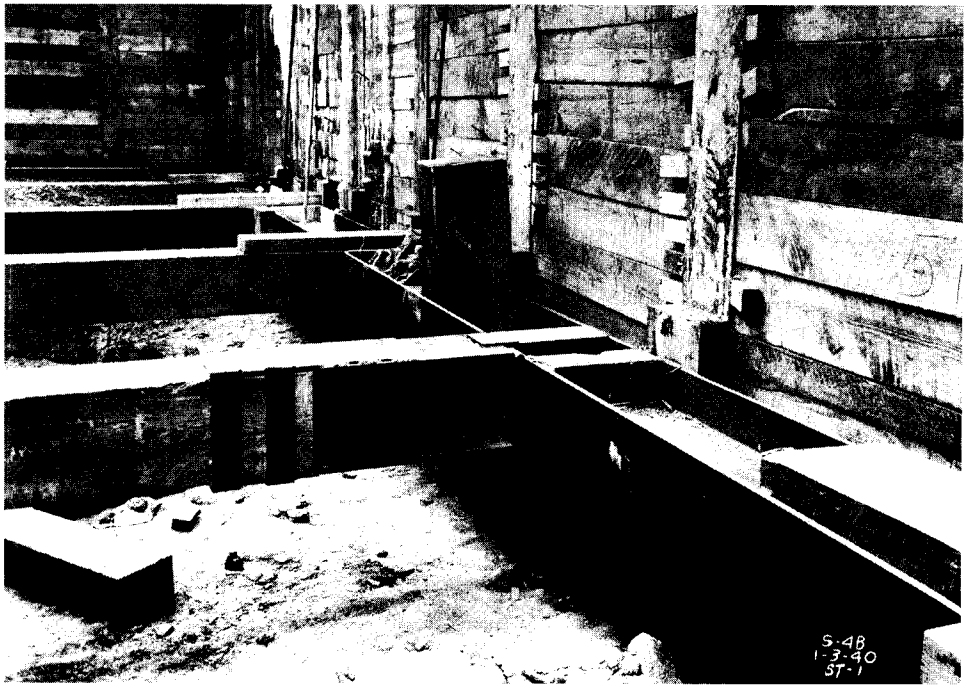

(a)

(b)

Figure 13.9 Braced cuts: (a) Chicago subway construction (courtesy of Ralph B. Peck); (b) in Seoul, South Korea (courtesy of E. C. Shin, University of Inchon, South Korea); (c) in Taiwan (courtesy of Richard Tsai, C&M Hi-Tech Engineering Co., Ltd., Taipei, Taiwan)

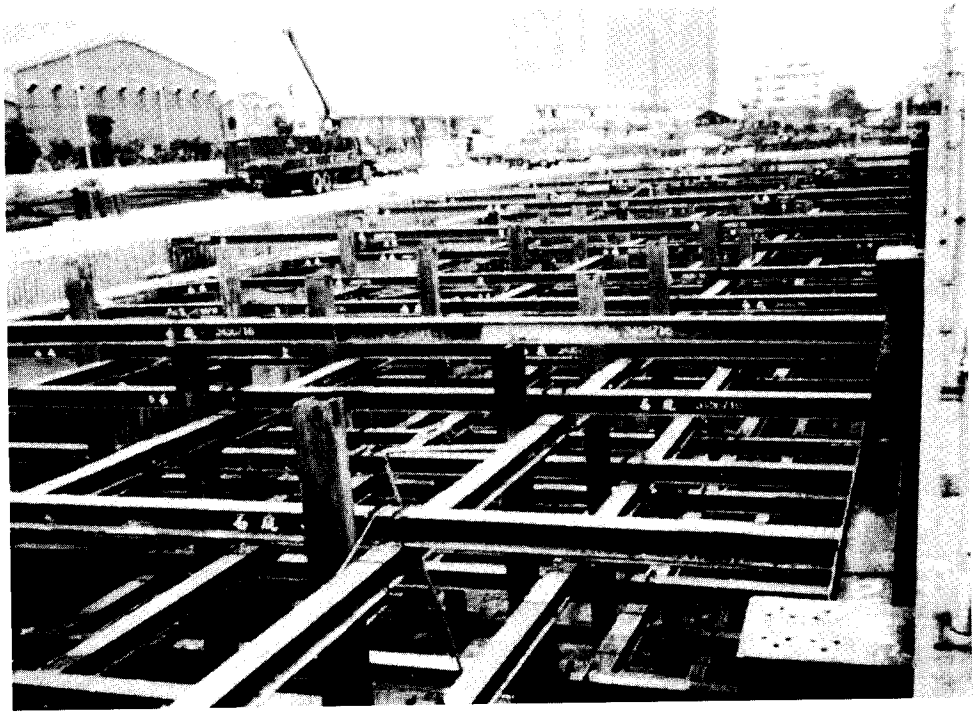

(c)

Figure 13.9 *(continued)*

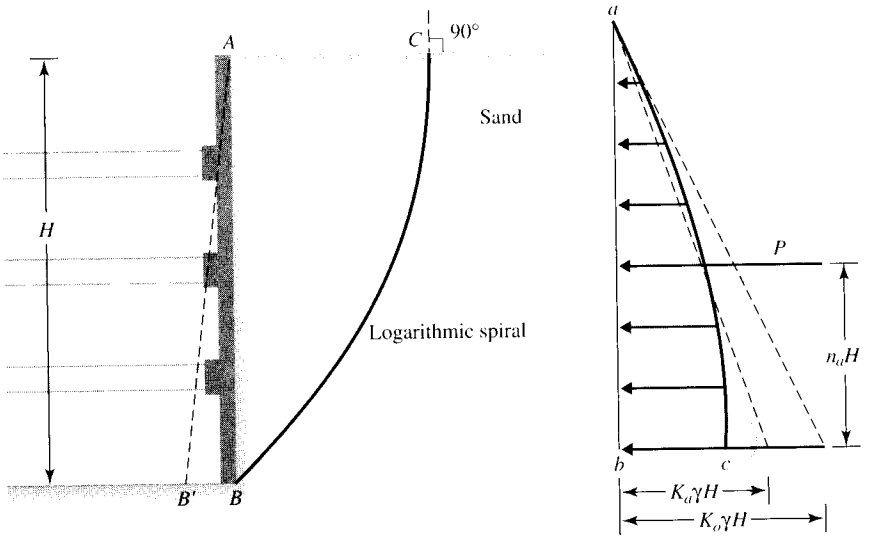

(a) (b)

Figure 13.10 Earth pressure distribution against a wall with rotation about the top

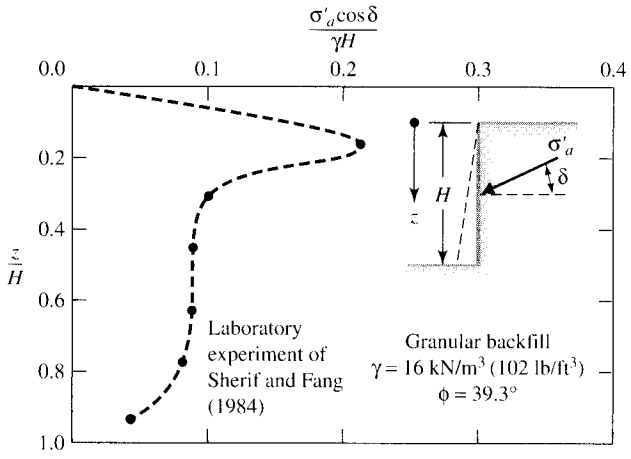

Figure 13.11
Laboratory observation of the distribution of horizontal component of lateral earth pressure on retaining wall rotating about the top.

Figure 13.11 shows the laboratory observations of Sherif and Fang (1984) related to the distribution of the horizontal component of the lateral earth pressure on a model retaining wall with a dry granular backfill rotating about the top. This figure clearly demonstrates the nonhydrostatic distribution of the lateral earth pressure for this type of wall movement.

13.7 Determination of Active Thrust on Bracing Systems of Open Cuts in Granular Soil

The active thrust on the bracing system of open cuts can be theoretically estimated by using trial wedges and Terzaghi's general wedge theory (1941). The basic procedure for determination of the active thrust are described in this section.

Figure 13.12a shows a braced wall AB of height H that deforms by rotating about its top. The wall is assumed to be rough, with the angle of wall friction equal to δ. The point of application of the active thrust (that is, $n_a H$) is assumed to be known. The curve of sliding is assumed to be an arc of a logarithmic spiral. As we discussed in the preceding section, the curve of sliding intersects the horizontal ground surface at 90°. To proceed with the trial wedge solution, let us select a point b_1. From b_1, a line $b_1 b'_1$ that makes an angle ϕ' with the ground surface is drawn. (Note that ϕ' = effective angle of friction of the soil.) The arc of the logarithmic spiral, $b_1 B$, which defines the curve of sliding for this trial, can now be drawn, with the center of the spiral (point O_1) located on the line $b_1 b'_1$. Note that the equation for the logarithmic spiral is given by $r_1 = r_o e^{\theta_1 \tan\phi'}$ and, in this case, $\overline{O_1 b_1} = r_o$ and $\overline{O_1 B} = r_1$. Also, it is interesting to see that the horizontal line that represents the ground surface is the normal to the curve of sliding at the point b_1, and that $O_1 b_1$ is a radial line. The angle between them is equal to ϕ', which agrees with the property of the spiral.

To look at the equilibrium of the failure wedge, let us consider the following forces per unit length of the braced wall:

1. W_1 = the weight of the wedge ABb_1 = (Area of ABb_1) × (γ) × (1).
2. P_1 = the active thrust acting at a point $n_a H$ measured vertically upward from the bottom of the cut and inclined at an angle δ with the horizontal.

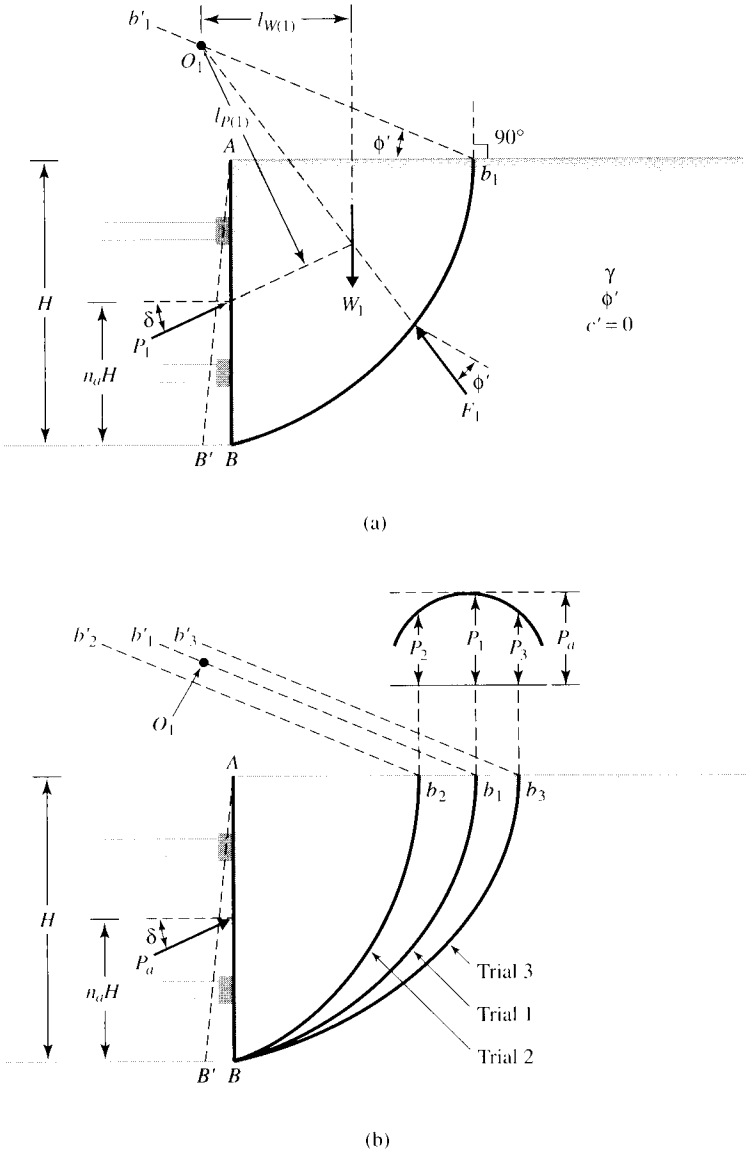

Figure 13.12
Determination of active force on bracing system of open cut in cohesionless soil

3. F_1 = the resultant of the shear and normal forces that act along the trial failure surface. The line of action of the force F_1 will pass through the point O_1.

Now, taking the moments of these forces about O_1, we have

$$W_1[l_{W(1)}] + F_1(0) - P_1[l_{P(1)}] = 0$$

or

$$P_1 = \frac{W_1 l_{W(1)}}{l_{P(1)}} \tag{13.13}$$

where $l_{W(1)}$ and $l_{P(1)}$ are the moment arms for the forces W_1 and P_1, respectively.

This procedure of finding the active thrust can now be repeated for several wedges such as ABb_2, ABb_3, . . ., ABb_n (Figure 13.12b). Note that the centers of the logarithmic spiral arcs will lie on lines b_2b_2', b_3b_3', . . ., b_nb_n', respectively. The active thrusts $P_1, P_2, P_3, \ldots, P_n$ derived from the trial wedges are plotted to some scale in the upper portion of Figure 13.12b. The maximum point of the smooth curve drawn through these points will yield the desired maximum active thrust, P_a, on the braced wall.

Kim and Preber (1969) determined the values of $P_a/0.5\gamma H^2$ for braced excavations for various values of ϕ', δ, and n_a. These values are given in Table 13.3. In general, the average magnitude of P_a is about 10% greater when the wall rotation is about the top as compared with the value obtained by Coulomb's active earth pressure theory.

Table 13.3 $P_a/0.5\gamma H^2$ Against ϕ', δ, and n_a ($c' = 0$) for Braced Cuts*

		$P_a/0.5\gamma H^2$						$P_a/0.5\gamma H^2$			
ϕ' (deg)	δ (deg)	$n_a = 0.3$	$n_a = 0.4$	$n_a = 0.5$	$n_a = 0.6$	ϕ' (deg)	δ (deg)	$n_a = 0.3$	$n_a = 0.4$	$n_a = 0.5$	$n_a = 0.6$
10	0	0.653	0.734	0.840	0.983	35	0	0.247	0.267	0.290	0.318
	5	0.623	0.700	0.799	0.933		5	0.239	0.258	0.280	0.318
	10	0.610	0.685	0.783	0.916		10	0.234	0.252	0.273	0.300
							15	0.231	0.249	0.270	0.296
15	0	0.542	0.602	0.679	0.778		20	0.231	0.248	0.269	0.295
	5	0.518	0.575	0.646	0.739		25	0.232	0.250	0.271	0.297
	10	0.505	0.559	0.629	0.719		30	0.236	0.254	0.276	0.302
	15	0.499	0.554	0.623	0.714		35	0.243	0.262	0.284	0.312
20	0	0.499	0.495	0.551	0.622	40	0	0.198	0.213	0.230	0.252
	5	0.430	0.473	0.526	0.593		5	0.192	0.206	0.223	0.244
	10	0.419	0.460	0.511	0.575		10	0.189	0.202	0.219	0.238
	15	0.413	0.454	0.504	0.568		15	0.187	0.200	0.216	0.236
	20	0.413	0.454	0.504	0.569		20	0.187	0.200	0.216	0.235
25	0	0.371	0.405	0.447	0.499		25	0.188	0.202	0.218	0.237
	5	0.356	0.389	0.428	0.477		30	0.192	0.205	0.222	0.241
	10	0.347	0.378	0.416	0.464		35	0.197	0.211	0.228	0.248
	15	0.342	0.373	0.410	0.457		40	0.205	0.220	0.237	0.259
	20	0.341	0.372	0.409	0.456						
	25	0.344	0.375	0.413	0.461	45	0	0.156	0.167	0.180	0.196
							5	0.152	0.163	0.175	0.190
30	0	0.304	0.330	0.361	0.400		10	0.150	0.160	0.172	0.187
	5	0.293	0.318	0.347	0.384		15	0.148	0.159	0.171	0.185
	10	0.286	0.310	0.339	0.374		20	0.149	0.159	0.171	0.185
	15	0.282	0.306	0.334	0.368		25	0.150	0.160	0.173	0.187
	20	0.281	0.305	0.332	0.367		30	0.153	0.164	0.176	0.190
	25	0.284	0.307	0.335	0.370		35	0.158	0.168	0.181	0.196
	30	0.289	0.313	0.341	0.377		40	0.164	0.175	0.188	0.204
							45	0.173	0.184	0.198	0.213

*After Kim and Preber (1969)

Table 13.4 Values of $P_a/0.5\gamma H^2$ for Cuts in a c'-ϕ' Soil with the Assumption $c_a = c'(\tan\delta/\tan\phi')$*

δ (deg)	$n_a = 0.3$ and $c'/\gamma H = 0.1$	$n_a = 0.4$ and $c'/\gamma H = 0.1$	$n_a = 0.5$ and $c'/\gamma H = 0.1$
$\phi' = 15°$			
0	0.254	0.285	0.322
5	0.214	0.240	0.270
10	0.187	0.210	0.238
15	0.169	0.191	0.218
$\phi' = 20°$			
0	0.191	0.210	0.236
5	0.160	0.179	0.200
10	0.140	0.156	0.173
15	0.122	0.127	0.154
20	0.113	0.124	0.140
$\phi' = 25°$			
0	0.138	0.150	0.167
5	0.116	0.128	0.141
10	0.099	0.110	0.122
15	0.085	0.095	0.106
20	0.074	0.083	0.093
25	0.065	0.074	0.083
$\phi' = 30°$			
0	0.093	0.103	0.113
5	0.078	0.086	0.094
10	0.066	0.073	0.080
15	0.056	0.060	0.067
20	0.047	0.051	0.056
25	0.036	0.042	0.047
30	0.029	0.033	0.038

*After Kim and Preber (1969)

13.8 Determination of Active Thrust on Bracing Systems for Cuts in Cohesive Soil

Using the principles of the general wedge theory, we can also determine the active thrust on bracing systems for cuts made in c'-ϕ' soil. Table 13.4 gives the variation of P_a in a nondimensional form for various values of ϕ', δ, n_a, and $c'/\gamma H$.

For the $\phi = 0$ condition, $c = c_u$. For this condition, it can be shown (Das and Seeley, 1975) that

$$P_a = \frac{1}{2(1 - n_a)}(0.677 - KN_c)\gamma H^2 \tag{13.14}$$

where

$$N_c = \left(\frac{c_u}{\gamma H}\right) \tag{13.15}$$

$$K = f\left(\frac{c_a}{c_u}\right) \tag{13.16}$$

where c_a = adhesion along the face of sheet piles.

The values of K are

$\left(\frac{c_a}{c_u}\right)$	K
0	2.762
0.5	3.056
1.0	3.143

13.9 Pressure Variation for Design of Sheetings, Struts, and Wales

The active thrust against sheeting in a braced cut, calculated by using the general wedge theory, does not explain the variation of the earth pressure with depth that is necessary for design work. An important difference between bracings in open cuts and retaining walls is that retaining walls fail as single units, whereas bracings in an open cut undergo progressive failure where one or more struts fail at one time.

Empirical lateral pressure diagrams against sheetings for the design of bracing systems have been given by Peck (1969). These pressure diagrams for cuts in sand, soft to medium clay, and stiff clay are given in Figure 13.13. Strut loads may be determined by assuming that the vertical members are hinged at each strut level except

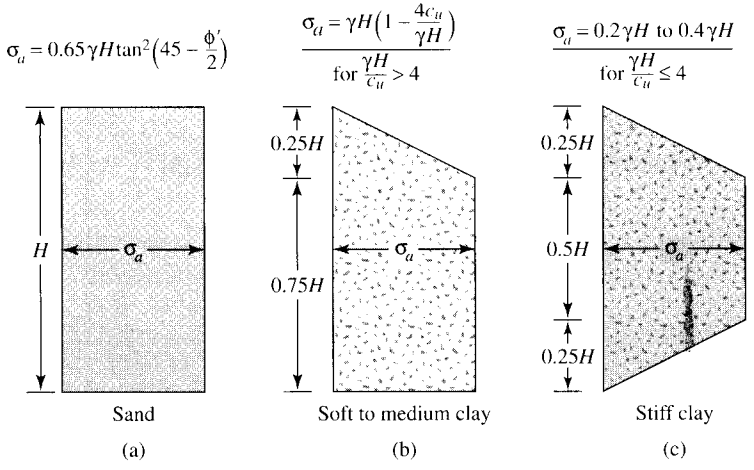

Figure 13.13 Peck's pressure diagrams for design of bracing systems

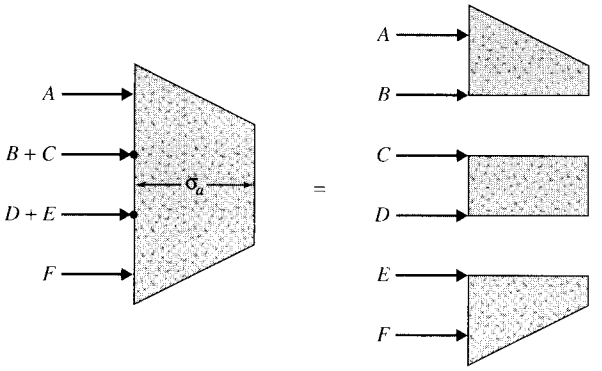

Figure 13.14 Determination of strut loads from empirical lateral pressure diagrams

the topmost and bottommost ones (Figure 13.14). Example 13.2 illustrates the procedure for the calculation of strut loads.

Example 13.2

A 7-m-deep braced cut in sand is shown in Figure 13.15. In the plan, the struts are placed at $s = 2$ m center to center. Using Peck's empirical pressure diagram, calculate the design strut loads.

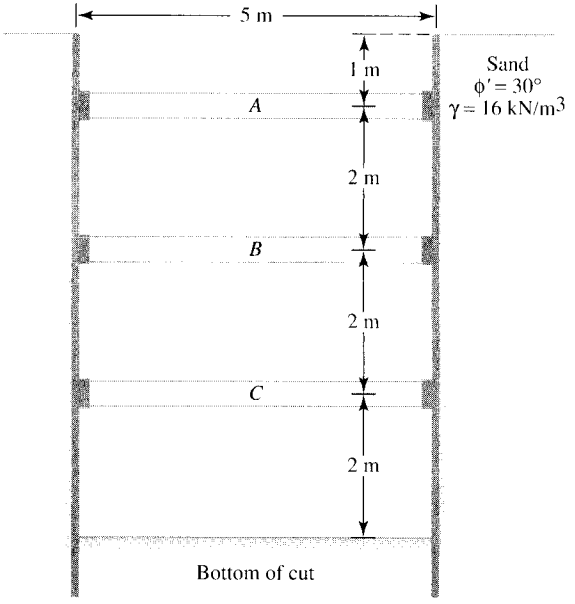

Figure 13.15 Braced cut in sand

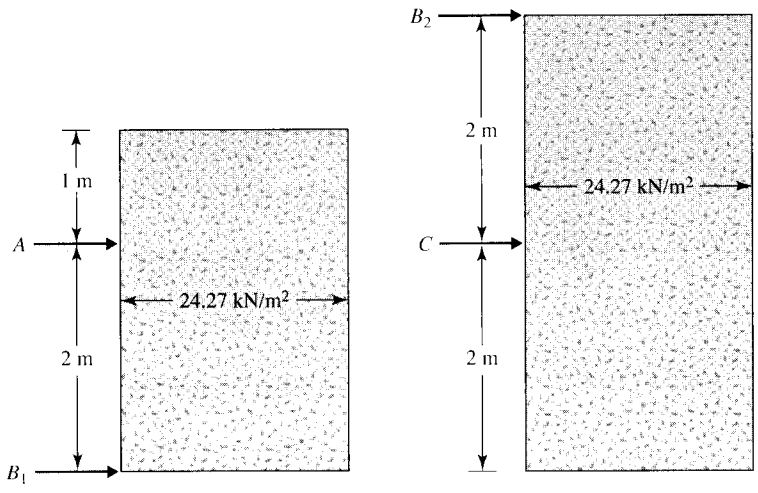

Figure 13.16 Calculation of strut loads from pressure envelope

Solution

Refer to Figure 13.13a. For the lateral earth pressure diagram,

$$\sigma_a = 0.65\gamma H \tan^2\left(45 - \frac{\phi'}{2}\right) = (0.65)(16)(7)\tan^2\left(45 - \frac{30}{2}\right) = 24.27 \text{ kN/m}^2$$

Assume that the sheeting is hinged at strut level B. Now refer to the diagram in Figure 13.16 We need to find reactions at A, B_1, B_2, and C. Taking the moment about B_1, we have

$$2A = (24.27)(3)(\tfrac{3}{2}); \qquad A = 54.61 \text{ kN/m}$$

Hence,

$$B_1 = (24.27)(3) - 54.61 = 18.2 \text{ kN/m}$$

Again, taking the moment about B_2, we have

$$2C = (24.27)(4)(\tfrac{4}{2})$$

$$C = 97.08 \text{ kN/m}$$

So

$$B_2 = (24.27)(4) - 97.08 = 0$$

The strut loads are as follows:

At level A: $(A)(s) = (54.61)(2) = \mathbf{109.22\ kN}$

At level B: $(B_1 + B_2)(s) = (18.2 + 0)(2) = \mathbf{36.4\ kN}$

At level C: $(C)(s) = (97.08)(2) = \mathbf{194.16\ kN}$ ■

13.10 Dynamic Earth Pressure Distribution Behind a Wall Rotating about the Top

Lateral earth pressure on braced cuts is essentially a problem in which the wall rotates about the top. On the basis of laboratory model test results, Sherif and Fang (1984) reported the dynamic earth pressure distribution behind a rigid retaining wall (H = 1 m) with dense sand as backfill material and rotation about its top. Figure 13.17 shows a plot of $\sigma'_a \cos\delta$ versus depth for various values of k_h (for $k_v = 0$). The magnitude of active thrust, P_{ae}, can be obtained from the equation

$$P_{ae}\cos\delta = \int_0^H (\sigma'_a \cos\delta)\, dz$$

or

$$P_{ae} = \frac{1}{\cos\delta}\int_0^H (\sigma'_a \cos\delta)\, dz \tag{13.17}$$

For a given value of k_h, the magnitude of P_{ae} is 15 to 20% higher than that obtained by using Eq. (12.72) (i.e., the case of wall rotation about the bottom).

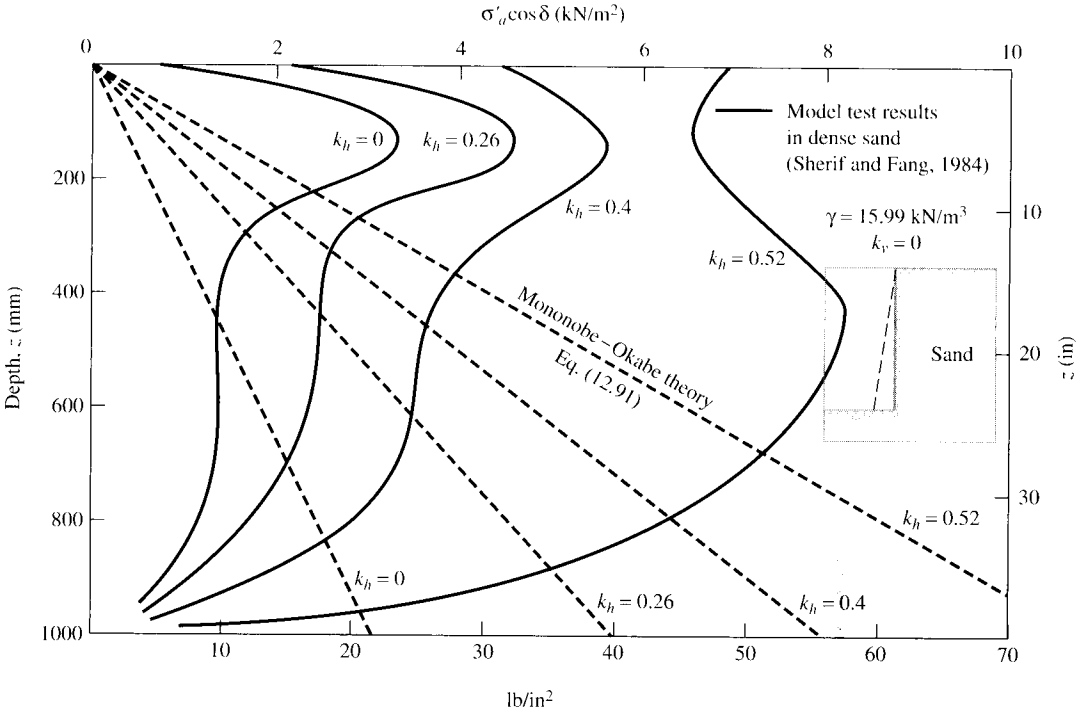

Figure 13.17 Dynamic lateral earth presure distribution behind a rigid model retaining wall rotating about the top

With the model test results just described, Sherif and Fang (1984) suggested that the location of the point of application of P_{ae} with the wall rotating about the top may be assumed to be $0.55H$ measured from the bottom of the wall.

13.11 Summary

This chapter covers two major topics: (a) estimation of passive pressure using curved failure surface in soil; and (b) lateral earth pressure on braced cuts using the general wedge theory and pressure envelopes for design of struts, wales, and sheet piles.

Passive pressure calculations using curved failure surface is essential for the case in which $\delta > \phi'/2$, since plane failure surface assumption provides results on the unsafe side for design.

In the case of braced cuts, although the general wedge theory provides the force per unit length of the cut, it does not provide the nature of distribution of earth pressure with depth. For that reason, pressure envelopes are necessary for practical design.

Problems

13.1 Draw a logarithmic spiral according to the equation $r = r_o e^{\theta \tan \phi'}$, with θ varying from 0° to 180°. Use $\phi' = 40°$ and $r_o = 30$ mm.

13.2 Refer to Figure 13.18. If $H = 6$ m, the density of soil (ρ) = 1850 kg/m^3, and the angle of wall friction (δ) = 17.5°, determine the passive force, P_p, per unit length of the wall. Use Caquot and Kerisel's solution.

13.3 Repeat Problem 13.2 with the following data: $H = 10$ ft, $\gamma = 110$ lb/ft^3, $\delta = 14°$.

13.4 A retaining wall has a vertical back face with a horizontal granular backfill. Given that

height of retaining wall = 15 ft
unit weight of soil = 100 lb/ft^3
soil friction angle, $\phi' = 30°$
$\delta = 2/3\ \phi'$,
$c' = 0$

calculate the passive force per foot length of the wall using Table 13.2.

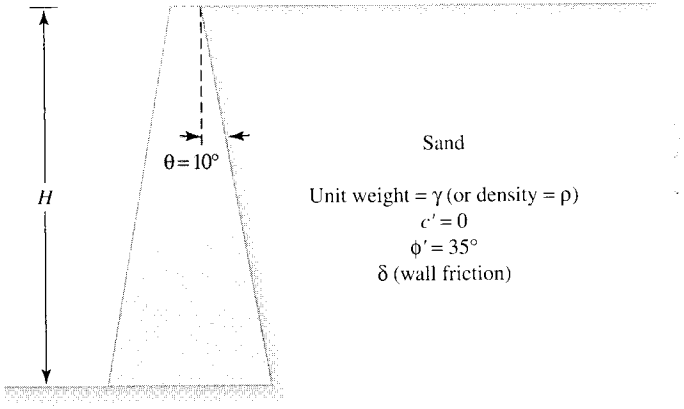

Figure 13.18

13.5 Refer to Figure 13.5. Given that $H = 5$ m, $\gamma = 16$ kN/m^3, $\phi' = 30°$, $\delta = 15°$, $k_v = 0$, and $k_h = 0.3$,
- **a.** Calculate P_{pe} for the retaining wall using the Mononobe–Okabe solution (Section 12.15);
- **b.** Calculate P_{pe} for the retaining wall using the logarithmic spiral solution (Section 13.5).

13.6 Using the theory described in the section on general wedge theory, determine the active thrust, P_a, for the braced wall shown in Figure 13.19.

13.7 The elevation and plan of a bracing system for an open cut in sand are shown in Figure 13.20. Assuming $\gamma_{sand} = 105$ lb/ft^3 and $\phi' = 38°$, determine the strut loads.

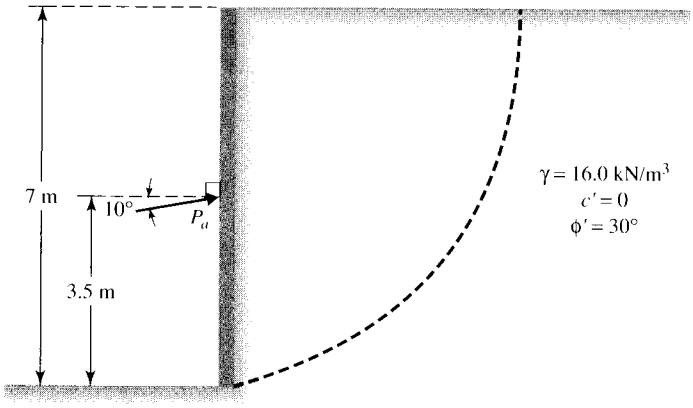

Figure 13.19

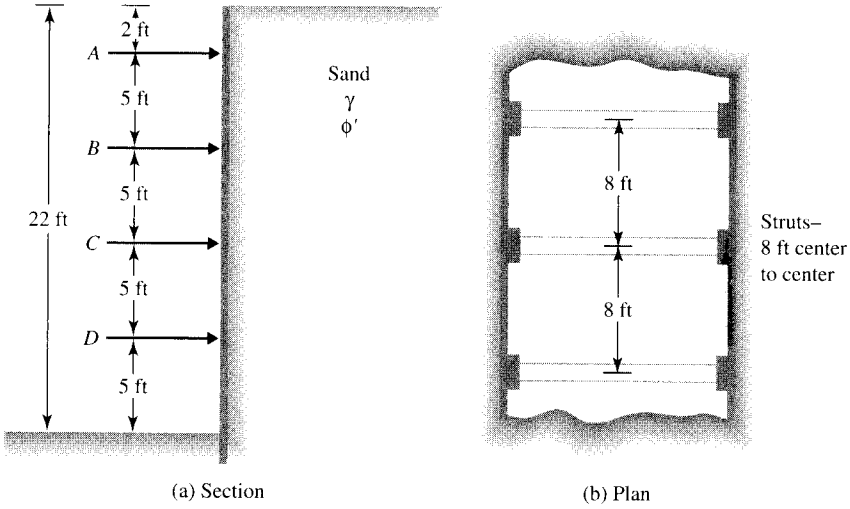

Figure 13.20

References

CAQUOT, A., and KERISEL, J. (1948). *Tables for the Calculation of Passive Pressure, Active Pressure, and Bearing Capacity of Foundations,* Gauthier-Villars, Paris.

DAS, B. M., and SEELEY, G. R. (1975). "Active Thrust on Braced Cut in Clay," *Journal of the Construction Division,* ASCE, Vol. 101, No. CO4, 945–949.

HIJAB, W. (1956). "A Note on the Centroid of a Logarithmic Spiral Sector," *Geotechnique,* Vol. 4, No. 2, 96–99.

KIM, J. S., and PREBER, T. (1969). "Earth Pressure Against Braced Excavations," *Journal of the Soil Mechanics and Foundations Division,* ASCE, Vol. 95, No. SM6, 1581–1584.

MORRISON, E. E., JR., and EBELING, R. M. (1995). "Limit Equilibrium Computation of Dynamic Passive Earth Pressure," *Canadian Geotechnical Journal,* Vol. 32, No. 3, 481–487.

PECK, R. B. (1969). "Deep Excavation and Tunneling in Soft Ground," *Proceedings,* 7th International Conference on Soil Mechanics and Foundation Engineering, Mexico City, State-of-the-Art Vol., 225–290.

SHERIF, M. A., and FANG, Y. S. (1984). "Dynamic Earth Pressure on Walls Rotating About the Top," *Soils and Foundations,* Vol. 24, No. 4, 109–117.

SHIELDS, D. H., and TOLUNAY, A. Z. (1973). "Passive Pressure Coefficients by Method of Slices," *Journal of the Soil Mechanics and Foundations Division,* ASCE, Vol. 99, No. SM12, 1043–1053.

TERZAGHI, K. (1941). "General Wedge Theory of Earth Pressure," *Transactions,* ASCE, Vol. 106, 68–97.

TERZAGHI, K., and PECK, R. B. (1967). *Soil Mechanics in Engineering Practice,* 2nd ed., Wiley, New York.